FULL TITLE
ASP Conference Series, Vol. **VOLUME**, **YEAR OF PUBLICATION**
NAMES OF EDITORS

The Advection of Supergranules by Large-Scale Flows

David H. Hathaway

NASA Marshall Space Flight Center, Huntsville, AL 35812 USA

Peter E. Williams, Manfred Cuntz

Department of Physics, University of Texas at Arlington, Arlington, TX 76019 USA

Abstract. We produce a 10-day series of simulated Doppler images at a 15-minute cadence that reproduces the spatial and temporal characteristics seen in the SOHO/MDI Doppler data. Our simulated data contains a spectrum of cellular flows with but two necessary components — a granule component that peaks at wavenumbers of about 4000 and a supergranule component that peaks at wavenumbers of about 110. We include the advection of these cellular components by a differential rotation profile that depends on latitude and wavenumber (depth). We further mimic the evolution of the cellular pattern by introducing random variations to the amplitudes and phases of the spectral components at rates that reproduce the level of cross-correlation as a function of time and latitude. Our simulated data do not include any wave-like characteristics for the supergranules yet can accurately reproduce the rotation characteristics previously attributed to wave-like characteristics.

1. Introduction

Supergranules are cellular flow structures observed in the solar photosphere with typical diameters of about 30 Mm and lifetimes of about one day. They cover the entire surface of the Sun and are intimately involved with the structure and evolution of the magnetic field in the photosphere. The magnetic structures of the chromospheric network form at the boundaries of these cells and magnetic elements are shuffled about the surface as the cells evolve. The diffusion of magnetic elements by the evolving supergranules has long been associated with the evolution of the Sun's magnetic field [Leighton (1964)].

Supergranules were discovered by Hart (1954). While these cellular flows were quickly identified as convective features [Leighton, Noyes, & Simon (1962)] the difficulty of detecting any associated thermal features consistent with that dentification (i.e. hot cell centers) has made this identification somewhat problematic [Worden (1975)].

The rotation of the supergranules has added further mystery to their nature. Duvall (1980) cross-correlated the equatorial Doppler velocity patterns and found that the supergranules rotated more rapidly than the plasma at the photosphere and that even faster rotation rates were obtained when longer (24-hour vs. 8-hour) time intervals were used. He attributed this behavior to a surface shear layer [proposed by Foukal & Jokipii (1975) and Foukal (1979) and modeled

by Gilman & Foukal (1979)] in which larger, longer-lived, cells extend deeper into the more rapidly rotating layers. Snodgrass & Ulrich (1990) used data from Mount Wilson Observatory to find the rotation rate at different latitudes and noted that the rotation rates for the Doppler pattern were some 4% faster than the spectroscopic rate and, more interestingly, some 2% faster than the magnetic features and sunspots. More recently Beck & Schou (2000) used a 2D Fourier transform method to find that the Doppler pattern rotates more rapidly than the shear layer itself and that larger features do rotate more rapidly than the smaller features. They suggested that supergranules have wave-like characteristics with a preference for prograde propagation.

In a previous paper [Hathaway, Williams, & Cuntz (2006)] we showed that this "super-rotation" of the Doppler pattern could be attributed to projection effects associated with the Doppler signal itself. As the velocity pattern rotates across the field of view its line-of-sight component is modulated in a way that essentially adds another half wave and gives a higher rotation rate that is a function of wavenumber. In that paper we took a fixed velocity pattern (which had spatial characteristics that matched the SOHO/MDI data) and rotated it rigidly to show this "super-rotation" effect. While this indicated that this Doppler projection effect should be accounted for, the fixed pattern could not account for all the variations reported by Beck & Schou (2000). Furthermore, when Schou (2003) "divided-out" the line-of-sight modulation he still saw prograde and retrograde moving components.

In this paper we report on our analyses of simulated data in which the supergranules are advected by a differential rotation that varies with both latitude and depth. The data is designed to faithfully mimic the SOHO/MDI data that was analyzed in Beck & Schou (2000) and Schou (2003) and the analyses are reproductions of those done in earlier studies.

2. The Data

The full-disk Doppler images from SOHO/MDI [Scherrer et al. (1995)] are obtained at a 1-minute cadence to resolve the temporal variations associated with the p-mode oscillations. We [c.f. Hathaway et al. (2000) and Beck & Schou (2000)] have temporally filtered the images to remove the p-mode signal by using a 31-minute long tapered Gaussian with a FWHM of 16 minutes on sets of 31 images that were de-rotated to register each to the central image. Series of these filtered images were formed at a 15-minute cadence over the 60-day MDI Dynamics Runs in 1996 and 1997. This filtering process effectively removes the p-mode signal and leaves behind the Doppler signal from flows with temporal variations longer than about 16 minutes. Supergranules, with typical wavenumbers of about 110, are very well resolved in this data (at disk center wavenumbers of about 1500 are resolved). While granules are not well resolved, they do appear in the data as pixel-to-pixel and image-to-image "noise," as a convective blue shift (due to the correlation between brightness and updrafts), and as resolved structures for the largest members.

The simulated data are constructed in the manner described in Hathaway (1988), Hathaway (1992), Hathaway et al. (2000), and Hathaway et al. (2002)

from vector velocities generated by an input spectrum of complex spectral coefficients for the radial, poloidal, and toroidal components.

To simulate the observed line-of-sight velocity the three vector velocity components are calculated on a grid with 1024 points in latitude and 2048 points in longitude. A Doppler velocity image is constructed by determining the longitude and latitude at a point on the image, finding the vector velocity at that point using bi-cubic interpolation, and then projecting that vector velocity onto the line-of-sight. The line-of-sight velocities at an array of 16 points within each pixel are determined and the average taken to simulate the integration over a pixel in the acquisition of the actual MDI Doppler data.

With the current simulations we have added two changes that were not included in our previous work on individual Doppler images. First, we add velocity "noise" at each pixel. This represents the contribution from the spatially unresolved granules that, nonetheless, have temporal varibility that is not filtered out by the 31-minute temporal filter. This noise has a center-to-limb variation due to the foreshortened area covered by each pixel and is randomly varied from pixel to pixel and from one Doppler image to the next. The noise level is determined by matching the initial drop in correlation from one image to the next that is seen in the MDI data. Secondly, we treat the instrumental blurring in a more realistic manner. Previously we took the Doppler velocity image and convolved it with an MDI point-spread-function. We now make red and blue intensity images from our Doppler velocity image and a simple limb darkened intensity image, convolve those with an MDI point-spread-function, and construct a blurred Doppler velocity image from the difference divided by the sum. This process yields a Doppler velocity image that is virtually indistinguishable from an MDI Doppler velocity image.

The velocity pattern is evolved in time by introducing changes to the spectral coefficients based on two processes - the advection by an axisymmetric zonal flow (differential rotation) and random processes that lead to the finite lifetime of the cells.

The advection by the differential rotation is governed by an advection equation

$$\frac{\partial u}{\partial t} = -\Omega(\theta)\frac{\partial u}{\partial \phi} \tag{1}$$

where u is a vector velocity component and $\Omega(\theta)$ is the differential rotation profile. We represent u as a series of spherical harmonic components and project this advection equation onto a single spherical harmonic which gives a series of coupled equations for the evolution of the spectral coefficients. Solid body rotation simply introduces a phase variation for each coefficient. Differential rotation couples the change in one spectral coefficient to spectral coefficients with wavenumbers $\ell \pm 2$ and $\ell \pm 4$ for differential rotation dependent on $\cos^2\theta$ and $\cos^4\theta$.

The finite lifetimes for the cells are simulated by introducing random perturbations to the spectral coefficient amplitudes and phases. The size of these perturbations increases with wavenumber to give shorter lifetimes to smaller cells.

3. The Analyses

Several anaylsis programs were applied to both the MDI data and the simulated data. Convection spectra for individual images were obtained using the methods described by Hathaway (1987) and Hathaway (1992) — the Doppler signal due to the motion of the observer is removed, the convective blue shift signal is identified and removed, the data is mapped to heliographic coordinates, the axisymmetric flow signals due to differential rotation and meridional circulation are identified and removed, and the remaining signal is projected onto spherical harmonics. The averaged spectra from the 1996 MDI Dynamics Run and from our 10-day simulated data run are nearly perfectly matched at all wavenumbers. This match is obtained by adjusting the input spectrum for the simulated data. This spectrum contains two Lorentzian-like spectral components — a supergranule component centered on $\ell \sim 110$ with a width of about 100 and a granule component centered on $\ell \sim 4000$ with a width of about 4000. The MDI spectrum is well matched with just these two components without the addition of a mesogranule component [November et al. (1981)]. In fact, we find a distinct *dip* in the spectrum at wavenumbers $\ell \sim 500$ that should be representative of mesogranules. This dip is also seen in spectra of the MDI high resolution data [Hathaway et al. (2000)].

Additional analyses are applied to the data after it has been mapped onto heliographic coordinates. Longitudal strips of this data centered on latitudes from 75° south to 75° north were cross-correlated with corresponding strips from later images as was done by Duvall (1980) and Snodgrass & Ulrich (1990). The longitudinal shift of the cross-correlation peak gives the rotation rate while the height of this peak is associated with cell lifetimes. These strips were also Fourier analyzed in longitude to get spectral coefficients and those coefficents were Fourier anaylzed in time over 10-day intervals as was done by Beck & Schou (2000) to get rotation rates as functions of wavenumber.

Fig. 1 shows the rotation rates from the cross-correlation analysis. The rotation profiles from the simulated data match those from the MDI data. Both show faster rotation rates for longer time lags as noted by Duvall (1980) and by Snodgrass & Ulrich (1990). This indicates that we have found the right latitudinal differential rotation profile.

The strength of the correlations as functions of latitude and time lag for both the MDI data and the simulated data are also well matched. This indicates that we have found the right lifetimes for the cells.

We have also reproduced the analysis of Schou (2003). The data strips are apodized and multiplied by longitude dependent functions designed to remove the Doppler projection effect and to isolate either longitudinal motions or latitudinal motions. The strips are shifted in longitude according to the differential rotation rate and then Fourier analysed in space and time to obtain "$k\omega$" diagrams.

Fig. 2A shows the equatorial rotation rate as a function of wavenumber for the simulated data while Fig. 2B shows the $k\omega$ diagram. These should be compared to Fig. 4 of Beck & Schou (2000) and Fig. 8 of Schou (2003) respectively.

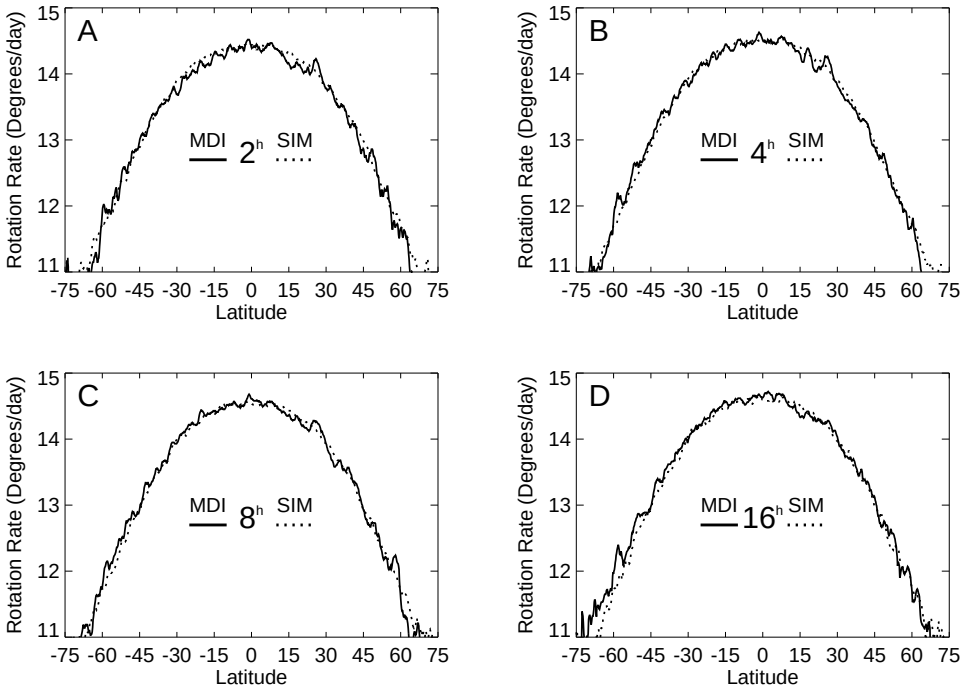

Figure 1. Rotation profiles from cross-correlation analyses of MDI data (solid lines) and simulated data (dotted lines). All profiles match at virtually all latitudes and time lags (Panel A — 2-hour, Panel B — 4-hour, Panel C — 8-hour, Panel D — 16-hour). Note that the measured equatorial rotation rate increases with time lag for both datasets.

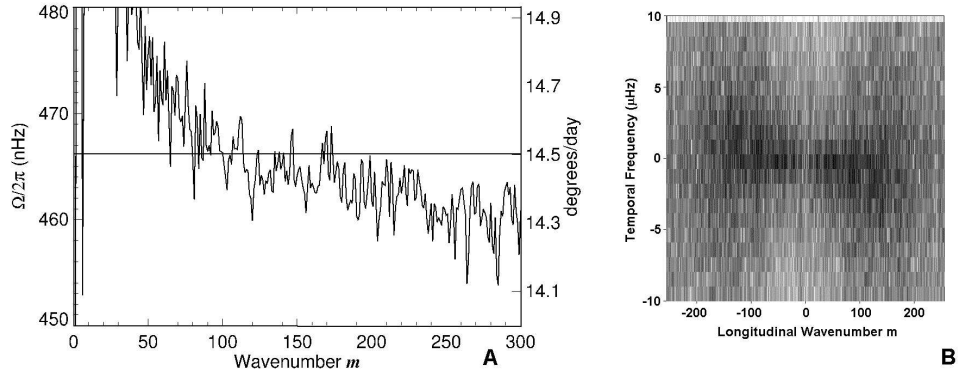

Figure 2. Panel A. The equatorial rotation rate as a function of wavenumber from our analysis of the simulated data showing the increase at small wavenumbers. Most of this increase is due to the Doppler velocity projection. Panel B. The $k\omega$ diagram from our analysis of the simulated data showing both prograde and retrograde moving elements. This spread in power is due to the random evolution of the cellular pattern.

4. Conclusions

We have produced simulated data in which the cellular structures (supergranules) are advected by differential rotation and evolve by uncorrelated random

changes. When we compare results from analyses of this data with those from analyses of the MDI data we find that the simulated data exhibits the same characteristics as the MDI data — the visual structures, the power spectra, the rotation characteristics, and the evolution rates all match. While some of these characteristics have been attributed to wave-like properties [c.f. Beck & Schou (2000) and Schou (2003)] our simulated data is simply advected by a zonal flow (differential rotation) with speeds that never exceed those determined from helioseismology [Schou et al. (1998)]. The differential rotation we impose does, however, have a dependence on wavenumber ℓ. If we assume that the rotation rate of cells with diameters, $D = 2\pi R_\odot/\ell$, reflects the rotation rate at a depth, $d = D/2$, then the surface shear layer indicated by our differential rotation has a thickness of about 20 Mm — somewhat thinner than the 30 Mm suggested by helioseismic inversions [Schou et al. (1998)].

Acknowledgments. We would like to thank NASA for its support of this research through a grant from the Heliophysics Guest Investigator Program to NASA Marshall Space Flight Center and The University of Texas Arlington. We would also like to thank the SOHO/MDI team for the critical role they played in producing the raw MDI data and John Beck in particular for implementing the temporal averaging of that data to remove the p-mode noise.

References

Beck, J. G., & Schou, J. 2000, Solar Phys., 193, 333
Duvall Jr., T. L. 1980, Solar Phys., 66, 213
Foukal, P. 1979, ApJ, 218, 539
Foukal, P., & Jokipii, R. 1975, ApJ, 199, L71
Gilman, P. A., & Foukal, P. 1979, ApJ, 229, 1179
Hart, A. B. 1954, MNRAS, 114, 17
Hathaway, D. H. 1987, Solar Phys., 108, 1
Hathaway, D. H. 1988, Solar Phys., 117, 329
Hathaway, D. H. 1992, Solar Phys., 137, 15
Hathaway, D. H., Beck, J. G., Bogart, R. S., Bachmann, K. T., Khatri, G., Petitto, J. M., Han, S., & Raymond, J. 2000, Solar Phys., 193, 299
Hathaway, D. H., Beck, J. G., Han, S., & Raymond, J. 2002, Solar Phys., 205, 25
Hathaway, D. H., Williams, P. E., & Cuntz,M. 2006, ApJ, 644, 598
Leighton, R. B. 1964, ApJ, 140, 1559
Leighton, R. B., Noyes, R. W., & Simon, G. W. 1962, ApJ, 135, 474
November, L. J., Toomre, J., Gebbie, K. B., and Simon, G. W. 1981, ApJ, 245, L123
Scherrer, P. H., Bogart, R. S., Bush, R. I., Hoeksema, J. T., Kosovichev, A. G., Schou, J., Rosenberg, W., Springer, L., Tarbell, T. D., Title, A., Wolfson, C. J., Zayer, I., and the MDI Engineering Team 1995, Solar Phys., 162, 129
Schou, J. 2003, ApJ, 596, L259
Schou, J., Antia, H. M., Basu, S., Bogart, R. S., Bush, R. I., Chitre, S. M., Christensen-Dalsgaard, J., Di Mauro, M. P., Dziembowski, W. A., Eff-Darwich, A., Gough, D. O., Haber, D. A., Hoeksema, J. T., Howe, R., Korzennik, S. G., Kosovichev, A. G., Larsen, R. M., Pijpers, F. P., Scherrer, P. H., Sekii, T., Tarbell, T. D., Title, A. M., Thompson, M. J., & Toomre, J. 1998, ApJ, 505, 390
Snodgrass, H. B., & Ulrich, R. K. 1990, ApJ, 351, 309
Worden, S. P. 1975, Solar Phys., 45, 521